Topological surface states on the nonpolar (110) and (111) surfaces of SmB_6

Dong-Choon Ryu,[1,*] Chang-Jong Kang,[2,*] Junwon Kim,[1,*] Kyoo Kim ⓘ,[1,3,†] G. Kotliar,[2,4]
J.-S. Kang,[5] J. D. Denlinger,[6,‡] and B. I. Min ⓘ[1,§]

[1]*Department of Physics, Pohang University of Science and Technology, Pohang 37673, Korea*
[2]*Department of Physics and Astronomy, Rutgers University, Piscataway, New Jersey 08854, USA*
[3]*MPPHC_CPM, Pohang University of Science and Technology, Pohang 37673, Korea*
[4]*Condensed Matter Physics and Materials Science Department,*
Brookhaven National Laboratory, Upton, New York 11973, USA
[5]*Department of Physics, The Catholic University of Korea, Bucheon 14662, Korea*
[6]*Advanced Light Source, Lawrence Berkeley Laboratory, Berkeley, California 94720, USA*

In order to clarify the controversial issue of the topological nature in a mixed-valent Kondo system, SmB_6, we have explored the surface states on the nonpolar (110) surface of SmB_6, employing both angle-resolved photoemission spectroscopy (ARPES) experiment and *ab initio* density-functional theory (DFT) band calculations. Based on ARPES spectroscopic fingerprints and the DFT surface band structures, we ascribe the observed spectral weights at $\bar{X}$ and $\bar{Y}$ on the (110) surface Brillouin zone to topological surface states (TSSs) of "topological insulator (TI)" nature and of "topological crystalline insulator (TCI)" nature, respectively. With varying the chemical potential, the double Dirac cones of the TCI nature exhibit a Lifshitz transition of Fermi surfaces with intriguing spin textures. We have also examined the TSSs on the nearly nonpolar (111) surface of SmB_6 in connection with a recently reported ARPES result and proposed a way to probe the Dirac points that are buried in the bulk-projected bands.

DOI: 10.1103/PhysRevB.103.125101

I. INTRODUCTION

Topological properties in strongly-correlated electron systems have been studied intensively in recent years [1,2]. Theoretical studies proposed that the topological nature in strongly correlated f-electron systems could emerge in conjunction with mixed-valent and Kondo physics [3,4], and angle-resolved photoemission spectroscopy (ARPES) experiments were conducted subsequently for a typical mixed-valent Kondo insulator SmB_6 to detect the proposed topological surface states (TSSs) [5–17]. However, the topological nature of SmB_6 is still controversial. While many ARPES groups reported that surface states are topological [10–15], some ARPES groups still reported that they are just trivial [16,17].

SmB_6 has the nontrivial Z_2 topology due to Sm $4f$-$5d$ band inversion in the bulk band structure, which is supposed to produce the gapless TSSs of Dirac-cone type on the (001) surface [18–21]. However, the Dirac points are buried in the bulk-projected bands, and so they have not been identified clearly in ARPES experiments yet. Since the (001) surface of simple-cubic SmB_6 has polar nature, it is not free from band bending and surface quantum-well confinement

in real experiments, which hampers the experimental verification of intrinsic topological properties [16]. Therefore, the investigation of the electronic structure on a nonpolar (110) surface of SmB_6 [see Fig. 1(a)] is demanded to corroborate the intrinsic topological nature of SmB_6, as was done for YbB_6 [22].

More controversies on the topological nature of SmB_6 are aroused by recent quantum oscillation measurements. One group [23] reported the observation of two-dimensional (2D)-like Fermi surfaces (FSs), supporting the TSSs, whereas the other group [24,25] reported the observation of 3D-like FSs that are as large as those of metallic LaB_6. Which one is intrinsic for SmB_6 is still under debate, but several exotic scenarios beyond Landau's Fermi-liquid theory were proposed to explain the anomalous features observed in the latter [26–29].

In this work, to address an interesting open question on the ground state of SmB_6, we have investigated the surface states in SmB_6 on its nonpolar (110) and also (111) surfaces, employing both ARPES experiment and density functional theory (DFT) band calculations. We have demonstrated that the (110) surface of SmB_6 hosts not only the TSSs of topological-insulator (TI) nature but also those of topological-crystalline-insulator (TCI) nature. We have shown that the emergence of TCI-type double Dirac cones in the latter are described well by the mirror Chern numbers (MCNs) for SmB_6 obtained from the model-independent *ab initio* band calculations. We have also confirmed that the (111) surface hosts the TSSs of TI character only. We propose a way to identify the Dirac points of TSSs that are buried under

* These authors contributed equally to this work.
† Present address: Korea Atomic Energy Research Institute (KAERI), 111 Daedeok-daero, Daejeon 34057, Korea.
‡ Corresponding author: JDDenlinger@lbl.gov
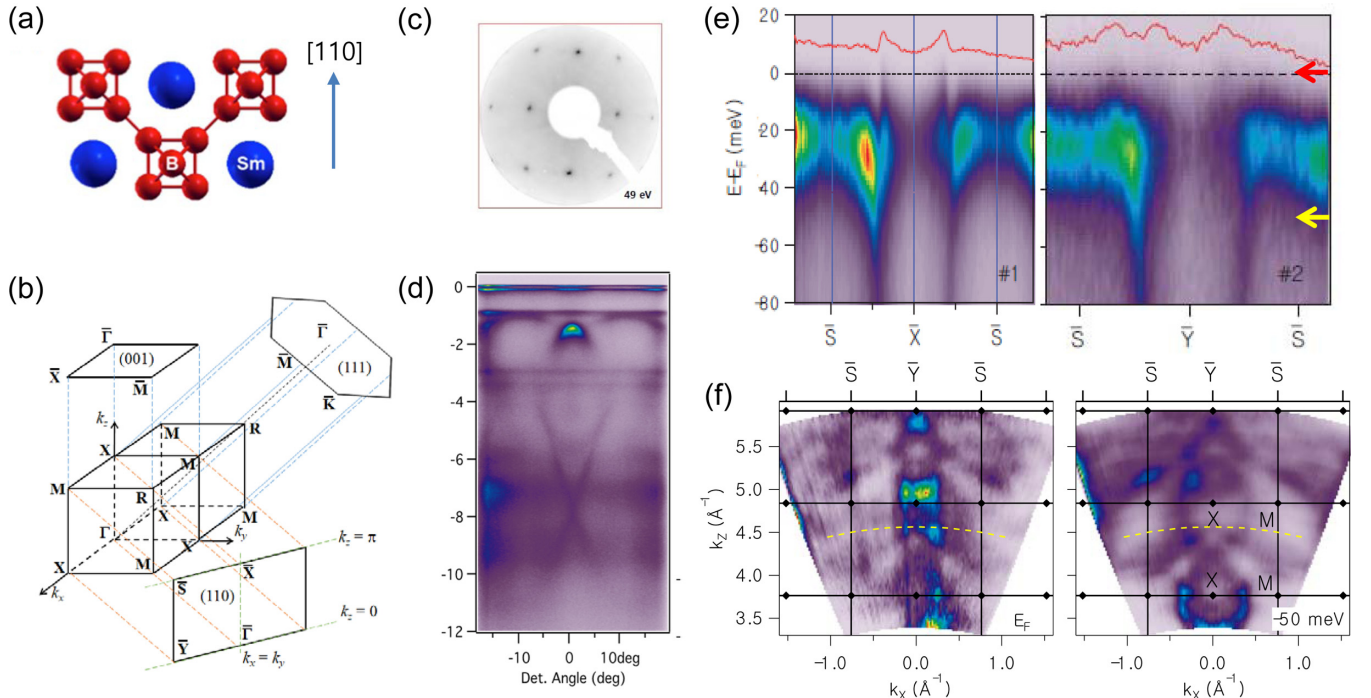§ Corresponding author: bimin@postech.ac.kr

FIG. 1. (a) Nonpolar (110) surface of SmB$_6$. (b) bulk and (001), (110), and (111) surface BZs of SmB$_6$. There are three mirror symmetry lines on the (110) surface: $\bar{\Gamma}$-$\bar{X}$, $\bar{\Gamma}$-$\bar{Y}$, and $\bar{X}$-$\bar{S}$. (c) LEED data of the prepared (110) surface of SmB$_6$. (d),(e) ARPES data for the (110) surface of SmB$_6$ obtained at 15 K using LV polarization. (d) Wide-energy-range dispersion images through $\bar{S}$-$\bar{Y}$-$\bar{S}$ measured at $h\nu = 70$ eV. (e) Near-E_F energy dispersion images through $\bar{S}$-$\bar{X}$-$\bar{S}$ measured at 66 eV and $\bar{S}$-$\bar{Y}$-$\bar{S}$ measured at 40 eV, respectively. Fermi-edge intensity line profiles (MDC at E_F in red) highlight the E_F-crossing in-gap states. Red-dotted and yellow-broken arrows denote the energy positions of E_F and -50 meV, respectively, at which angle-dependent CE maps were measured (see Fig. 3 below). (f) Photon-dependent map ($h\nu = 30$–120 eV) at the (110) surface BZ boundary ($k_y = 0.54$ Å^{-1}) with E_F and -50 meV energy slices, showing 2D vertical $\bar{Y}$ states and 3D bulk states around X and M, respectively. Dotted arcs correspond to the angle map energy, shown in Fig. 3(a).

the bulk-projected bands, which can be utilized possibly in ARPES experiment.

II. EXPERIMENTAL AND COMPUTATIONAL DETAILS

The (110) surface of SmB$_6$ was prepared by polishing a Laue-oriented single crystal followed by *in-vacuum* ion sputtering and high temperature (T) annealing to 1300 °C. ARPES measurements were performed at the MERLIN beamline 4.0.3 at the Advanced Light Source (ALS), using a Scienta R8000 electron energy analyzer and a low T six-axis sample manipulator cooled with an open-cycle He flow cryostat.

To investigate surface electronic structures, we have constructed the Wannierized tight-binding (TB) Hamiltonian from *ab initio* DFT bulk band results [30–33] and performed semi-infinite TB slab calculations [34–36]. It is noteworthy that the shapes of DFT band structures near the Fermi level (E_F) are essentially the same as those obtained by the dynamical mean-field theory (DMFT) at low temperature (T) below the coherence temperature (T_{coh}), suggesting that the strong correlation effect of $4f$ electrons in Kondo systems can be captured by renormalizing DFT $4f$ bands with a proper scale factor [13,20,21,37]. The topological nature of surface states is analyzed in terms of the MCNs, obtained from the Wilson-loop calculations [38–42]. Computational details are provided in the Supplemental Material (SM) [43].

III. RESULTS AND DISCUSSIONS

Figure 1(c) shows the measured low-energy electron diffraction (LEED) pattern of the (110) surface of SmB$_6$, which confirmed the formation of 1×1 rectangular long-range surface order with the $\sqrt{2}$ aspect ratio. Figures 1(d) and 1(e) show ARPES data obtained at 15 K using linear-vertical (LV) polarization of the incident photons. The wide energy range ARPES spectra through $\bar{S}$-$\bar{Y}$-$\bar{S}$ at $h\nu = 70$ eV in Fig. 1(d) reveal both dispersive bands and several k-independent multiplets between -2 eV and -12 eV. Here the dispersive bands are primarily of B $2p$ character, while k-independent streaks correspond to the Sm $4f^4$ ($-12 \sim -6$ eV) and Sm $4f^5$ (-2 eV $\sim E_F$) final state multiplets (see Fig. 2 in Ref. [44]). These LEED pattern and good-quality wide ARPES spectra in Figs. 1(c) and 1(d) confirm that the prepared (110) surface of SmB$_6$ is clean and well ordered, representing the intrinsic SmB$_6$ (110) surface.

Figure 1(e) shows the near-E_F ARPES spectra through $\bar{S}$-$\bar{X}$-$\bar{S}$ measured at 66 eV and $\bar{S}$-$\bar{Y}$-$\bar{S}$ measured at 40 eV, respectively, with the momentum-distribution curves (MDCs) denoted in red. Here the MDCs of the Fermi-edge intensity line profiles are shown to highlight the E_F-crossing in-gap states. For both cases, the flat bands of mainly $4f$ states exist in common at around -20 meV. Also the in-gap surface states cutting E_F are apparent around $\bar{X}$ and $\bar{Y}$ in ARPES (see the MDC peaks near $\bar{X}$ and $\bar{Y}$), in good agreement with theoretical
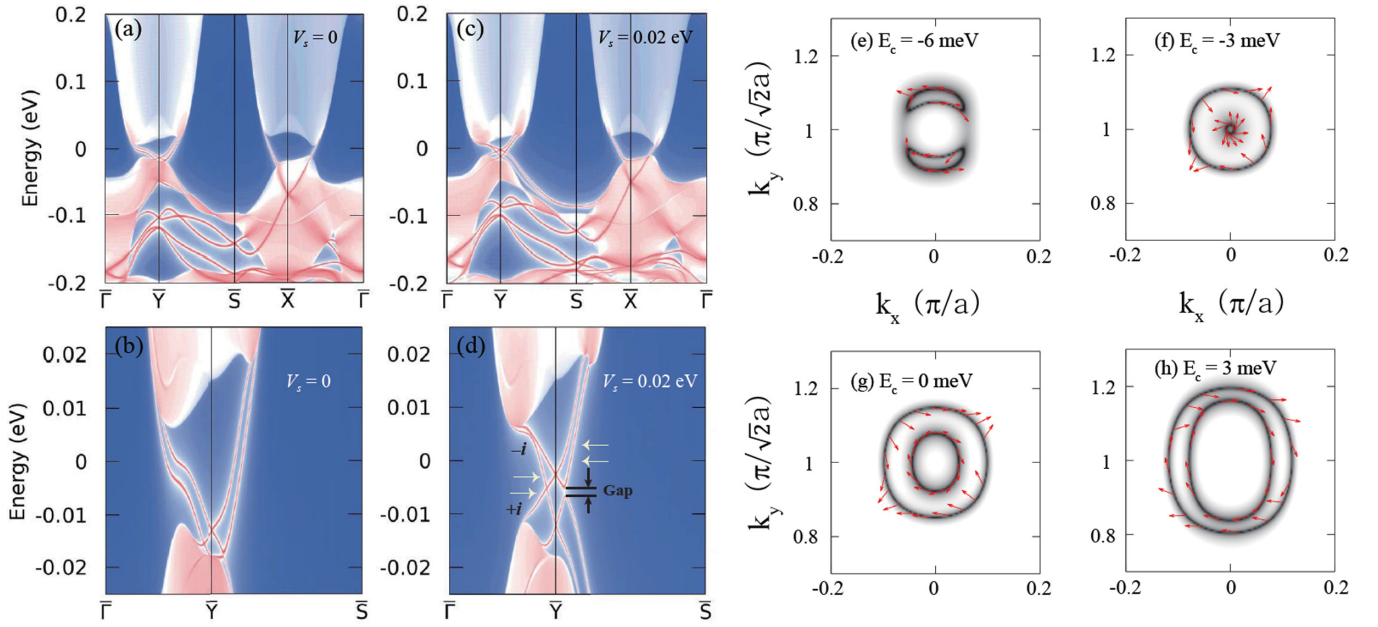
FIG. 2. (a),(b) Band structures for the (110) surface of SmB_6 with the surface potential $V_s = 0$, and (c),(d) those with $V_s = 0.02$ eV. The double Dirac-cone surface states near $\bar{Y}$ in (a) and (c) are magnified in (b) and (d). Dirac point along $\bar{\Gamma}$-$\bar{Y}$ and the gap opening along $\bar{Y}$-$\bar{S}$ are clearly visible in (d). Opposite mirror eigenvalues ($+i$ and $-i$) protect the band crossing along $\bar{\Gamma}$-$\bar{Y}$. (e)–(h) Constant-energy (CE) surfaces centered at $\bar{Y}$ as a function of energy cut (E_c) denoted by white arrow for the (110) surface with $V_s = 0.02$ eV, which exhibits a Lifshitz transition of FS's. Spin texture for each CE surface reveals either the Dresselhaus type [(e)–(g)] or the Rashba type (h), depending on E_c. When compared with experimental results, the DFT energy values in (a)–(h) should be rescaled by a factor of $1/10$, which is estimated by the quasiparticle weight at E_F from the DMFT self-energy of the $4f$ electrons [20].

results of Fig. 2(a) below, even though the existence of Dirac band crossings is not manifested well in ARPES. The nature of surface states at E_F can be identified by using the photon energy map shown in Fig. 1(f). In contrast to the dispersive 3D character of bulk bands at -50 meV (right), the bands at E_F around $\bar{Y}$ show clear vertical streaks (left), indicating their 2D surface character.

Figure 2(a) shows the band structures for the (110) surface of SmB_6 obtained by semi-infinite TB slab calculations based on the Wannierized model of DFT bulk band structures. We have checked that the results of semi-infinite TB slab calculations are qualitatively consistent with those of *ab initio* DFT slab calculations. Namely, the (110) surface band structure in Fig. 2(a) is consistent with that of DFT slab calculation shown in Fig. S1 of the SM [43].

For the (110) surface of SmB_6, two nonequivalent X points of bulk BZ are projected onto $\bar{Y}$ of surface BZ, and X and R points of bulk BZ are projected onto $\bar{X}$ of surface BZ, as shown in Fig. 1(b). As a result, double Dirac cones and a single Dirac cone are realized at $\bar{Y}$ and $\bar{X}$, respectively, as shown in Fig. 2(a). Then the double Dirac cones at $\bar{Y}$ could hybridize each other to produce a hybridization gap. The single Dirac cone realized at $\bar{X}$ is buried inside the bulk-projected bands and so only the upper part of the Dirac cone is shown in the gap region. On the other hand, as shown in Fig. 2(b), Dirac points arising from the double Dirac cones near $\bar{Y}$ just touch the bulk-projected bands.

To see the Dirac points more clearly in the gap region, we adjusted the surface onsite potential V_s manually in the TB slab calculations. When V_s is changed from 0 to 0.02 eV, the double Dirac cones near $\bar{Y}$ are shifted up in the gap region, as shown in Figs. 2(c) and 2(d). It is clearly shown in Fig. 2(d) that, while the band crossing along $\bar{Y}$-$\bar{S}$ is split to have a gap, along $\bar{\Gamma}$-$\bar{Y}$ is protected. Note that there are mirror-symmetry lines on the (110) surface, $\bar{\Gamma}$-$\bar{X}$, $\bar{\Gamma}$-$\bar{Y}$, and $\bar{X}$-$\bar{S}$ lines, originating from the mirror-symmetry planes possessed in the bulk BZ of SmB_6. Since the surface states along $\bar{\Gamma}$-$\bar{Y}$ have opposite mirror eigenvalues ($+i$ and $-i$), the band crossing is symmetry protected [38,39,42]. Then a Dirac point could be realized in between $\bar{\Gamma}$ and $\bar{Y}$ (see also Fig. S2(a) in the SM [43]). In contrast, the band crossing along $\bar{Y}$-$\bar{S}$ is not symmetry protected so as to produce a gap, as shown in Fig. 2(d) and Fig. S2(b). The emergence of these intriguing TSSs is reminiscent of those realized in a TCI system of SnTe [45]. Therefore, the (110) surface of SmB_6 hosts the TSSs of both TI (at $\bar{X}$) and TCI (around $\bar{Y}$) nature, which is in marked in contrast to the (001) and (111) surfaces (see Fig. 4 below) that host the Dirac cones of TI nature only.

Figures 2(e)–2(h) show the constant-energy (CE) surfaces on the (110) surface of SmB_6 with $V_s = 0.02$ eV. Interestingly, with increasing the energy cut (E_c) in Fig. 2(d), the shape of CE surfaces centered at $\bar{Y}$ is changed topologically, from crescent type (e) to double-elliptical type (h). This is indeed a topological Lifshitz transition, which has been addressed in characterizing the TCI nature [45]. The spin textures on the CE surfaces of (110) surface reveal the spin-momentum locking behaviors, which provides another evidence for the topological nature of SmB_6. It is notable that the spin texture varies with varying E_c, displaying both the Dresselhaus-type and the Rashba-type spin textures [39,40].
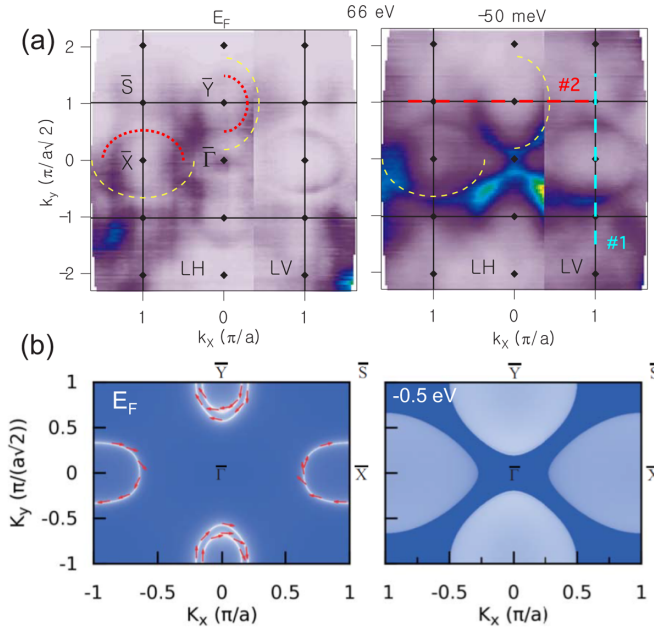
FIG. 3. (a) Angle-dependent (k_x-k_y) CE maps for the (110) surface of SmB$_6$ obtained at 66 eV with energy slices at E_F (red dotted) and −50 meV (yellow broken), using both LH and LV polarization, respectively. Broken lines #1 and #2 correspond to EDC image cuts in Fig. 1(e). (b) Theoretical FS with spin helicity (left) and CE map at −0.5 eV (right). For the comparison between theory and experiment, one needs to take into account the scale factor of 1/10 in the DFT 4f-band width due to the band renormalization effect [20]. Namely, the DFT energy −0.5 eV in (b) would correspond to the ARPES energy −50 meV in (a).

Note that, when moving around the CE contour counterclockwise, the spin direction rotates clockwise for the Dresselhaus type but counterclockwise for the Rashba type. In this context, the spin textures on the CE contours in Figs. 2(e) and 2(h) are of Dresselhaus type and of Rashba type, respectively.
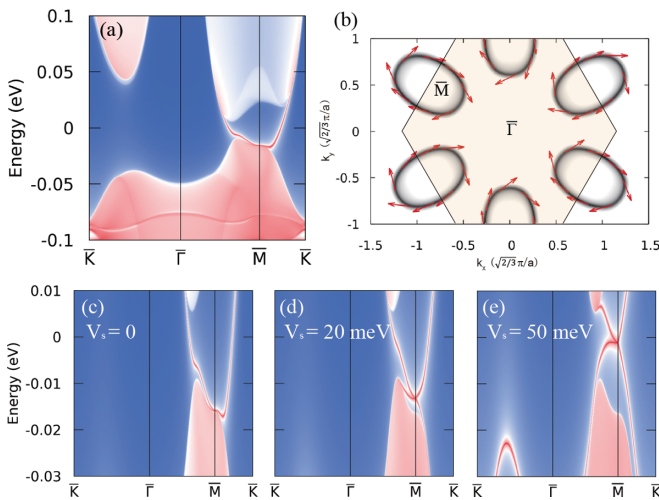

FIG. 4. (a) Band structure and (b) FS for the (111) surface of SmB$_6$ with B$_6$ termination. (c)–(e) (111) surface band structures for different surface potential V_s.

Intriguingly, however, the spin textures on the outer and inner contours in Figs. 2(f) and 2(g) are different, namely the outer one being of Dresselhaus type and the inner one being of Rashba type.

We have applied the Wilson-loop method to calculate three distinct mirror Chern numbers (MCNs): $C_0 \equiv C_{k_z=0}^+$, $C_\pi \equiv C_{k_z=\pi}^+$, and $C_d \equiv C_{k_x=k_y}^+$, which are mirror invariant under the $k_z = 0$, $k_z = \pi$, and $k_x = k_y$ mirror planes, respectively. Here the superscript + denotes the MCN having a mirror eigenvalue of $+i$. As a result, $(C_0, C_\pi, C_d) = (+2, +1, -1)$ is obtained, as shown in Fig. S3 in the SM [43]. Here $C_0 = 2$ is consistent with the existence of two Dirac cones along the $\bar{Y}$-$\bar{\Gamma}$-$\bar{Y}$ mirror-symmetry line.

Figure 3(a) shows the FS (red-dotted lines) and the CE map at −50 meV (yellow-broken lines) for the (110) surface of SmB$_6$, which are clearly identified in both linear-horizontal (LH) and LV polarization ARPES's. Note that the FS and the CE map in Fig. 3(a) are well matched with theoretical ones in Fig. 3(b), albeit the latter are a bit smaller than the former. In theoretical FS, there are single and double FS's centered at $\bar{X}$ and $\bar{Y}$, respectively, and both FS's have the Rashba-type spin textures. In ARPES, however, whether the FS's centered at $\bar{Y}$ are really double or not is not clearly resolved. Nevertheless, the MDC peaks of surface states around $\bar{Y}$ in Fig. 1(e) are seen to be broader than those around $\bar{X}$. Since the dispersions of the bands at $\bar{X}$ and $\bar{Y}$ are similar, the broadness of the spectral weights at $\bar{Y}$ highly suggests the existence of double FSs. Moreover, considering that the number of Dirac points should be odd on any surface BZ of a strong TI SmB$_6$, the FS's centered at $\bar{Y}$ in ARPES are supposed to be double.

We have also explored the TSSs on the (111) surface of SmB$_6$. For the (111) surface of SmB$_6$, the X point of bulk BZ is projected onto $\bar{M}$ of surface BZ [see Fig. 1(b)], and so a single Dirac cone is expected at $\bar{M}$. Figure 4(a) shows the surface band structure of (111) surface of SmB$_6$ with B$_6$ termination [46]. Indeed the TSSs are realized at $\bar{M}$. We have checked that the surface band structure for the Sm termination is quite similar to that for the B$_6$ termination. As shown in Fig. 4(a), the Dirac points here too are almost buried in the bulk-projected bands, and so they would be hard to be detected in ARPES. Shown in Fig. 4(b) are the FSs for the (111) surface of SmB$_6$ with B$_6$ termination. There appear electron pocket FSs centered at $\bar{M}$. Recent ARPES measurement on the (111) surface of SmB$_6$ also shows $\bar{M}$-centered electron pockets with the Rashba-type spin helicity as in Fig. 4(b), but the size of observed Fermi surfaces is a bit bigger [47].

As shown above, the Dirac points on all three surfaces of SmB$_6$ are buried under the bulk-projected bands, and so the identification of them in ARPES would be extremely hard. Earlier, in Figs. 2(c) and 2(d), we saw that the surface potential V_s shifts the surface chemical potential so as to locate the band crossings in the gap region. This feature suggests that the Dirac points could also be realized in the gap region by adjusting V_s. Indeed, as shown in Figs. 4(c)–4(e), the Dirac point at $\bar{M}$ on the (111) surface is shifted up in the gap region with increasing V_s, which indicates that the Dirac points can be identified in ARPES by applying the surface potential. In the band calculation, the surface potential is just a constant energy shift of the surface band energy. In the experiment, such an

effect can be realized by hole doping at the surface. One way is to dope divalent Yb or Ca at the surface Sm sites [48]. The other way is dosing halogen elements like F or Cl at the surface [49], as in dosing alkali metals for the electron doping. It is thus quite worthwhile to do ARPES experiment on such prepared samples of SmB_6.

We have demonstrated that the nonpolar (110) surface of SmB_6 hosts the TSSs of TCI nature in addition to those of TI nature, whereby a topological Lifshitz transition takes place with intriguing spin-texture variation. We have also explored the TSSs on the nearly nonpolar (111) surface of SmB_6 and proposed a way to detect the Dirac points that are buried in the bulk-projected bands via ARPES. Further experimental proof is thus urgently demanded to identify intriguing features of the double Dirac cones of TCI nature on the (110) surface of SmB_6 as well as the regular Dirac points of TI

nature on the (111) surface of properly prepared samples of SmB_6.

[1] M. Z. Hasan and C. L. Kane, Rev. Mod. Phys. **82**, 3045 (2010).

[2] X.-L. Qi and S.-C. Zhang, Rev. Mod. Phys. **83**, 1057 (2011).

[3] M. Dzero, K. Sun, V. Galitski, and P. Coleman, Phys. Rev. Lett. **104**, 106408 (2010).

[4] M. Dzero, K. Sun, P. Coleman, and V. Galitski, Phys. Rev. B **85**, 045130 (2012).

[5] S. Wolgast, Ç. Kurdak, K. Sun, J. W. Allen, D.-J. Kim, and Z. Fisk, Phys. Rev. B **88**, 180405(R) (2013).

[6] D. J. Kim, S. Thomas, T. Grant, J. Botimer, Z. Fisk, and J. Xia, Sci. Rep. **3**, 3150 (2013).

[7] D. J. Kim, J. Xia, and Z. Fisk, Nat. Mater. **13**, 466 (2014).

[8] S. Rößer, T.-H. Jang, D.-J. Kim, L. H. Tjeng, Z. Fisk, F. Steglich, and S. Wirth, Proc. Natl. Acad. Sci. USA **111**, 4798 (2014).

[9] L. Jiao, S. Rößer, D. J. Kim, L. H. Tjeng, Z. Fisk, F. Steglich, and S. Wirth, Nat. Commun. **7**, 13762 (2016).

[10] N. Xu, X. Shi, P. K. Biswas, C. E. Matt, R. S. Dhaka, Y. Huang, N. C. Plumb, M. Radović, J. H. Dil, E. Pomjakushina, K. Conder, A. Amato, Z. Salman, D. McK. Paul, J. Mesot, H. Ding, and M. Shi, Phys. Rev. B **88**, 121102(R) (2013).

[11] J. Jiang, S. Li, T. Zhang, Z. Sun, F. Chen, Z. R. Ye, M. Xu, Q. Q. Ge, S. Y. Tan, X. H. Niu, M. Xia, B. P. Xie, Y. F. Li, X. H. Chen, H. H. Wen, and D. L. Feng, Nat. Commun. **4**, 3010 (2013).

[12] M. Neupane, N. Alidoust, S.-Y. Xu, T. Kondo, Y. Ishida, D. J. Kim, C. Liu, I. Belopolski, Y. J. Jo, T.-R. Chang, H.-T. Jeng, T. Durakiewicz, L. Balicas, H. Lin, A. Bansil, S. Shin, Z. Fisk, and M. Z. Hasan, Nat. Commun. **4**, 2991 (2013).

[13] J. D. Denlinger, J. W. Allen, J.-S. Kang, K. Sun, J.-W. Kim, J. H. Shim, B. I. Min, D.-J. Kim, and Z. Fisk, arXiv:1312.6637.

[14] C.-H. Min, P. Lutz, S. Fiedler, B. Y. Kang, B. K. Cho, H.-D. Kim, H. Bentmann, and F. Reinert, Phys. Rev. Lett. **112**, 226402 (2014).

[15] N. Xu, P. K. Biswas, J. H. Dil, R. S. Dhaka, G. Landolt, S. Muff, C. E. Matt, X. Shi, N. C. Plimb, M. Radović, E. Pomjakushina, K. Conder, A. Amato, S. V. Borisenko, R. Yu, H.-M. Weng, Z. Fang, X. Dai, J. Mesot, H. Ding, and M. Shi, Nat. Commun. **5**, 4566 (2014).

[16] Z.-H. Zhu, A. Nicolaou, G. Levy, N. P. Butch, P. Syers, X. F. Wang, J. Paglione, G. A. Sawatzky, I. S. Elfimov, and A. Damascelli, Phys. Rev. Lett. **111**, 216402 (2013).

[17] P. Hlawenka, K. Siemensmeyer, E. Weschke, A. Varykhalov, J. Sánchez-Barriga, N. Y. Shitsevalova, A. V. Dukhnenko, V. B. Filipov, S. Gabáni, K. Flachbart, O. Rader, and E. D. L. Rienks, Nat. Commun. **9**, 517 (2018).

[18] T. Takimoto, J. Phys. Soc. Jpn. **80**, 123710 (2011).

[19] F. Lu, J. Z. Zhao, H. Weng, Z. Fang, and X. Dai, Phys. Rev. Lett. **110**, 096401 (2013).

[20] J. Kim, K. Kim, C.-J. Kang, S. Kim, H. C. Choi, J.-S. Kang, J. D. Denlinger, and B. I. Min, Phys. Rev. B **90**, 075131 (2014).

[21] C.-J. Kang, J. Kim, K. Kim, J. Kang, J. D. Denlinger, and B. I. Min, J. Phys. Soc. Jpn. **84**, 024722 (2015).

[22] C.-J. Kang, J. D. Denlinger, J. W. Allen, C.-H. Min, F. Reinert, B. Y. Kang, B. K. Cho, J.-S. Kang, J. H. Shim, and B. I. Min, Phys. Rev. Lett. **116**, 116401 (2016).

[23] G. Li, Z. Xiang, F. Yu, T. Asaba, B. Lawson, P. Cai, C. Tinsman, A. Berkley, S. Wolgast, Y. S. Eo, D.-J. Kim, C. Kurdak, J. W. Allen, K. Sun, X. H. Chen, Y. Y. Wangm, Z. Fisk, and L. Li, Science **346**, 1208 (2014).

[24] B. S. Tan, Y.-T. Hsu, B. Zeng, M. C. Hatnean, N. Harrison, Z. Zhu, M. Hartstein, M. Kiourlappou, A. Sirvastava, M. D. Johannes, T. P. Murphy, J.-H. Park, L. Balicas, G. G. Lonzarich, G. Balakrishnan, and S. E. Sebastian, Science **349**, 287 (2015).

[25] M. Hartstein, W. H. Toews, Y.-T. Hsu, B. Zeng, X. Chen, M. C. Hatnean, Q. R. Zhang, S. Nakamura, A. S. Padgett, G. Rodway-Gant, J. Berk, M. K. Kingston, G. H. Zhang, M. K. Chan, S. Yamashita, T. Sakakibara, Y. Takano, J.-H. Park, L. Balicas, N. Harrison *et al.*, Nat. Phys. **14**, 166 (2018).

[26] J. Knolle and N. R. Cooper, Phys. Rev. Lett. **118**, 096604 (2017).

[27] O. Erten, P.-Y. Chang, P. Coleman, and A. M. Tsvelik, Phys. Rev. Lett. **119**, 057603 (2017).

[28] D. Chowdhury, I. Sodemann, and T. Senthil, Nat. Commun. **9**, 1866 (2018).

[29] L. Li, K. Sun, C. Kurdak, and J. W. Allen, Nat. Rev. Phys. **2**, 463 (2020).

[30] G. Kresse and D. Joubert, Phys. Rev. B **59**, 1758 (1999).

[31] G. Kresse and J. Furthmüller, Phys. Rev. B **54**, 11169 (1996); Comput. Mater. Sci. **6**, 15 (1996).

[32] J. P. Perdew, K. Burke, and M. Ernzerhof, Phys. Rev. Lett. **77**, 3865 (1996).

[33] P. Blaha, K. Schwarz, G. K. H. Madsen, D. Kvasnicka, and J. Luitz, *WIEN2K* (Karlheinz Schwarz, Technische Universitat Wien, Austria, 2001).

[34] A. A. Mostofi, J. R. Yates, G. Pizzi, Y. S. Lee, I. Souza, D. Vanderbilt, and N. Marzari, Comput. Phys. Commun. **185**, 2309 (2014).

[35] M. P. Lopez Sancho, J. M. Lopez Sancho, and J. Rubio, J. Phys. F: Met. Phys. **15**, 851 (1985).

[36] Q. S. Wu, S. N. Zhang, H.-F. Song, M. Troyer, and A. A. Soluyanov, Comput. Phys. Commun. **224**, 405 (2018).

[37] C.-J. Kang, H. C. Choi, K. Kim, and B. I. Min, Phys. Rev. Lett. **114**, 166404 (2015).

[38] M. Ye, J. W. Allen, and K. Sun, arXiv:1307.7191.

[39] M. Legner, A. Rüegg, and M. Sigrist, Phys. Rev. Lett. **115**, 156405 (2015).

[40] P. P. Baruselli and M. Vojta, Phys. Rev. Lett. **115**, 156404 (2015).

[41] P. P. Baruselli and M. Vojta, Phys. Rev. B **93**, 195117 (2016).

[42] M. Legner, A. Rüegg, and M. Sigrist, Phys. Rev. B **89**, 085110 (2014).

[43] See Supplemental Material at http://link.aps.org/supplemental/10.1103/PhysRevB.103.125101 for the computational details,

band structures, and FSs from the *ab initio* DFT slab calculation for the (110) surface of SmB_6 (Fig. S1), mirror eigenvalues for the (110) surface of SmB_6 (Fig. S2), MCNs for SmB_6 obtained from the Wilson-loop calculations (Fig. S3), and the (111) surface structure of SmB_6 (Fig. S4).

[44] J. D. Denlinger, J. W. Allen, J.-S. Kang, K. Sun, B. I. Min, D.-J. Kim, and Z. Fisk, JPS Conf. Proc. **3**, 017038 (2014).

[45] T. H. Hsieh, H. Lin, J. Liu, W. Duan, A. Bansil, and L. Fu, Nat. Commun. **3**, 982 (2012).

[46] The (111) surface of SmB_6 would have two different terminations, because Sm and the center of the B_6 cage are not in the same plane, and so the (111) surface is not completely nonpolar (see Fig. S4 in the Supplemental Material).

[47] Y. Ohtsubo, Y. Yamashita, K. Hagiwara, S. Ideta, K. Tanaka, R. Yukawa, K. Horiba, H. Kumigashira, K. Miyamoto, T. Okuda, W. Hirano, F. Iga, and S. Kimura, Nat. Commun. **10**, 2298 (2019).

[48] S. Gabani, M. Orendac, G. Pristas, E. Gazo, P. Diko, S. Piovarci, V. Glushkov, N. Sluchanko, A. Levchenko, N. Shitsevalova, and K. Flachbart, Philos. Mag. **96**, 3274 (2016).

[49] H. Zhu, W. Zhou, and J. A. Yarmoff, J. Phys. Chem. C **122**, 16122 (2018).